Penerbit Akademia Baru

Journal of Advanced Research Design

Journal homepage:
https://akademiabaru.com/submit/index.php/ard
ISSN: 2289-7984

Effective Periodic Noise Reduction for Ship Corrosion Image

Md Mahadi Hasan Imran[1], Shahrizan Jamaludin[1,*], Mohammed Ismail Russtam Suhrab[2], Md Ibnul Hasan[3], Md Aman Ullah[3], Ahmad Ali Imran Mohd Ali[1], Ahmad Faisal Mohamad Ayob[1], Mohd Faizal Ali Akhbar[1], Mohamad Riduan Ramli[4], Farhana Arzu[5]

[1] Program of Maritime Technology and Naval Architecture, Faculty of Ocean Engineering Technology, Universiti Malaysia Terengganu, 21030 Kuala Nerus, Terengganu, Malaysia
[2] Faculty of Maritime Studies, Universiti Malaysia Terengganu, 21030 Kuala Nerus, Terengganu, Malaysia
[3] Faculty of Computer Science and Mathematics, Universiti Malaysia Terengganu, 21030 Kuala Nerus, Terengganu, Malaysia
[4] Faculty of Marine Engineering, Malaysia Maritime Academy, 78200 Kuala Sungai Baru, Melaka, Malaysia
[5] Department of Harbour and River Engineering, Faculty of Engineering and Technology, Bangabandhu Sheikh Mujibur Rahman Maritime University, 1216 Dhaka, Bangladesh

ARTICLE INFO

Article history:
Received 22 November 2024
Received in revised form 10 December 2024
Accepted 7 April 2025
Available online 30 April 2025

Keywords:
Periodic noise; corrosion images; gaussian notch reject filter; image de-nosing; high accuracy

ABSTRACT

Marine corrosion research has recently applied advanced image processing techniques. However, the investigation might have been interrupted due to the frequent disruption of corrosion images by certain noises, leading to a significant reduction in analysis accuracy. The comprehensive investigation of corrosion images required the implementation of progressive noise reduction techniques, especially for addressing periodic noise. Hence, the primary objective of this research is to investigate the reduction of periodic noise in ship corrosion images by leveraging a state-of-the-art image processing technique known as the Modified Gaussian Notch-Reject Filter (MGNRF). The methodology includes the selection of noise frequency using a window-based approach and the application of MGNRF for noise reduction. In comparison to other algorithms, the proposed algorithm has achieved promising results, with a mean absolute error (MAE) of 1.287, a remarkable average peak signal-to-noise ratio (PSNR) value of 40.215 and an exceptionally high mean structural similarity index (MSSIM) value of 0.998. This demonstrates the efficiency of the proposed algorithm in efficiently reducing periodic noise and enhancing the quality of ship corrosion images, thus ensuring accurate analysis and making a significant contribution to this critical domain.

1. Introduction

Image acquisition encompasses the process of obtaining a digitized image from a real-world source, yet various factors can introduce undesired alterations to the image pixels, commonly referred to as "noise" [1-3]. Within this realm of image noise, periodic noise stands out as a particularly troublesome subtype, introducing repetitive and sporadic patterns into digital images, affecting the entire image with burst-like disturbances, thus complicating its separation from the

* *Corresponding author*
E-mail address: shahrizanj@umt.edu.my

https://doi.org/10.37934/ard.129.1.130147

intended content within the spatial domain [4,5]. In the frequency domain, periodic noise manifests as high-amplitude spikes corresponding to the noise's frequency components with origins ranging from electrical and electromechanical interference during image capture to thermal instability in optical components, variations in electronic circuit gain in optical sensors and even scanning processes in electro-optical scanners [6-9].

An illustrative example of periodic noise's impact is its potential to corrupt imaging system outputs installed on oscillating support structures, as seen in unstable helicopters or affect television receivers when encountering weak signals or electrical interference, such as inter-harmonics from the power supply frequency [10,11]. Periodic noises are typically expressed by Chakraborty *et al.,* [12] as the cumulative sum of 'S' sinusoidal components in the spatial domain, as shown in Eq. (1).

$$n(x,y) = \sum_{i=1}^{S} A_i \sin[2\pi u_{0_i} \left(x + P_{x_i}\right) + 2\pi v_{0_i} \left(y + P_{y_i}\right)] \quad (1)$$

Where, S = number of sinusoids in spatial domain. A = amplitude, u_{0_i} and v_{0_i} = determine the sinusoidal frequencies. P_{x_i} and P_{y_i} = Phase displacement.

The pervasiveness of periodic noise is evident across various visual applications, including fields like medicine [13], remote sensing [14,15], television [16], traffic control [13], canvas contamination, [17] and real-time applications. Furthermore, image processing approaches have gained are widespread use in maritime industry including, encompassing corrosion detection, structural failure prediction, coating assessment, oil and gas pipe inspection and other ship maintenance strategies [18-21]. However, these approaches face significant interferences from various form of noise, specifically, periodic noise, characterized by repetitive patterns, poses a substantial challenge by degrading image quality [22]. Additionally, postures a risk to the image's suitability for subsequent processing tasks like image un-mixing and classification.

Periodic noise in ship corrosion images is caused by various external factors including, vibrations, lighting conditions, electrical interference, resulting in possibility of misinterpreting corrosion pattern [23]. The existence of periodic noise in corrosion images is a consistence issues that effects the reliability and efficiency of the corrosion assessment methods [19]. A comprehensive assessment is essential for preserving the structural integrity, operational efficiency of maritime assets, safety, while also minimizing the maintenance costs [24]. Therefore, addressing periodic noise is essential not only for enhancing the visual appeal of images but also for ensuring their accuracy and utility in corrosion assessment.

The purpose of this research is to meticulously evaluate and establish the efficacy of the Modified Gaussian Notch-Reject Filter (MGNRF) in mitigating periodic noise within ship corrosion images, thereby significantly elevating the precision and uniformity of corrosion evaluations. This endeavour introduces a transformative approach in the realm of image processing applied to maritime infrastructure maintenance, showcasing a method that adeptly confronts the intricacies posed by periodic noise in the context of corrosion detection or other corrosion assessments.

By ingeniously customizing the Gaussian Notch-Reject Filter to meet the unique demands of maritime conditions, this study unveils a solution that is remarkable for its versatility across varying noise intensities. This characteristic is crucial within the maritime industry, where the quality of corrosion imagery is directly correlated with the effectiveness of maintenance planning and the assurance of structural safety. The enhanced detection accuracy brought about by the MGNRF heralds a new era in corrosion assessment, promising more dependable evaluations that could lead to smarter, cost-effective maintenance strategies and, ultimately, safer maritime operations.

2. Literature Review

The literature presents a rich history of research efforts directed towards mitigating periodic noise in digital images. Notably, in 1963, Guttman *et al.,* [25] introduced the concept of periodicity, laying the foundation for subsequent investigations into this enduring challenge, highlighting the continuous contributions to advancing image processing techniques.

Periodic noise is typically categorized into three primary types: global periodic noise, local periodic noise and stripping patterns, as indicated by sources [26,27]. Global periodic noise represents repetitive, unwanted patterns with fixed characteristics affecting the entire image. It predominantly stems from the interference of independent periodic signals, like the potential impact of adjacent digital clock signals on image sensor devices or the interference of periodic digital signals with analogue TV sets. On the other hand, local periodic noise exhibits variability in its parameters, such as frequency, amplitude and phase, contingent upon the image's relative coordinates. This form of noise can be attributed to differences in sensitivity among detectors and their associated electronic circuits in multi-sensor imaging systems. Stripping patterns, the third category of periodic noise, are characterized by the presence of periodic stripes. These stripes' period is typically determined by the number of detectors within the imaging device. Another source of striping noise can be traced to the interference arising from fluctuations in the light intensity of 50 (60Hz) fluorescent lamps with the rolling shutter mechanism of an image sensor. To facilitate a clearer understanding of these three distinct types of periodic noise, Figure 1 provides a visual representation.

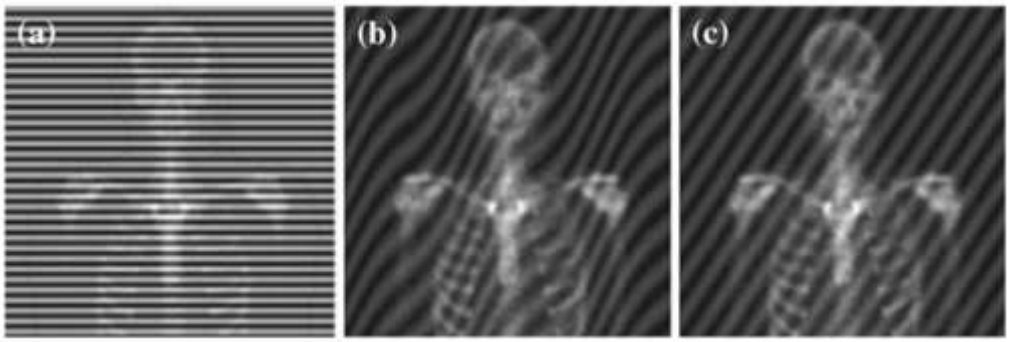

Fig. 1. Types of noise contamination in x-ray images of the human skeleton, contaminated by (a) stripping (b) local (c) global periodic noise [28]

With the ubiquitous presence of periodic noise in various imaging processes, it becomes imperative to incorporate a periodic noise elimination phase as a pre-processing step in utmost computer vision and image processing applications. Periodic noise reduction methods can be broadly categorized into two main groups: spatial methods and spectral methods. Spatial methods are particularly suitable for addressing stripping noise, which is comparatively simpler to manage in the spatial domain than other forms of periodic noise. Spatial domain techniques work directly with the image pixels to eliminate or reduce periodic noise. These methods are applied directly to the pixel values in the image and do not involve transformations to the frequency domain, making them suitable for addressing noise that is primarily manifested in the spatial arrangement of pixels [29,51]. In contrast, spectral methods rely on frequency domain filtering techniques to tackle periodic noise issues [30]. These two categories offer distinct approaches to mitigating periodic noise, each with its advantages and limitations. Figure 2 provides a visual representation of these periodic noise reduction methods. Following sections, a brief existing literature are demonstrated. Subsequent

sections will delve into the existing literature to provide a concise overview of the field's current state.

In 2002, Mean Filter Spectral Domain (MFS1) was introduced as a technique designed to address noise-affected spectral components. This was accomplished by employing a local mask mean values as a static notch filter to alleviate the noise's influence [31]. In a similar vein, the Median Filter in Spectral Domain (MFS2) was devised for reducing periodic and quasi-periodic noises, with its method focusing on identifying a frequency as noisy if the ratio of the local masked median of frequencies, obtained through scanning a local window, exceeded a predefined threshold [32]. On the other hand, alternative approaches, namely the frequency domain mean filter (FDMF1) [31], frequency domain median filter (FDMF2) [32] and other algorithms, employ static windows of fixed sizes to address noisy areas noisy areas but lack adaptability in pinpointing the positions of noisy peaks. Hudhud *et al.,* [33] employs a non-automated procedure to identify noisy peaks. In contrast, the FDMF1, FDMF2, Windowed Gaussian Notch Filter (WGNF), Gaussian star filter (GSF) and AONF algorithms utilize automated procedures for locating the central noisy peak. However, these algorithms tend to misclassify noise detection when applied to noisy peak areas that coincide with strong periodic noise falling within the low-frequency regions (LFRs) of the Fourier-transformed image.

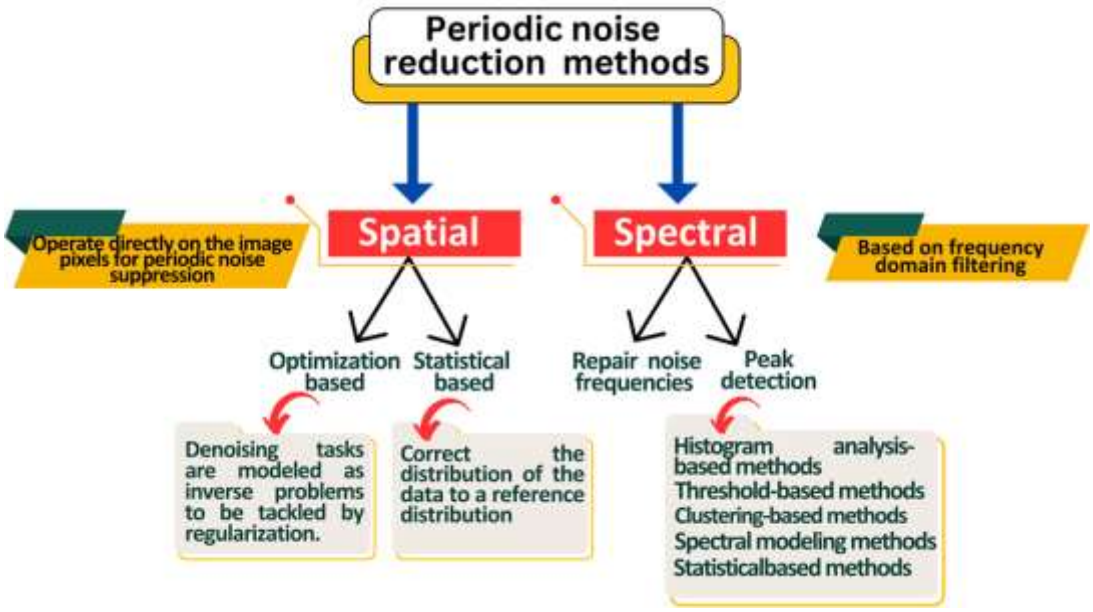

Fig. 2. Periodic noise reduction methods

Efficient WGNF was employed by Aizenberg *et al.,* [34] for detecting and filtering periodic/quasi-periodic noise. This approach detected noisy peaks, initially detected using MFS2 [32] and then filtered them with an improved version of the ideal Gaussian Notch Reject Filter (GNRF) [35]. However, because of the use of a fixed window size and predefined coefficients for the gaussian notch filter, this process may not consistently produce optimal restoration results.

Konstantinidis *et al.,* [36] proposed a practical solution for addressing periodic patterns induced by electromagnetic interference in Complementary Metal Oxide Semiconductor (CMOS) active pixel sensors within dual energy imaging. Their approach involved a semi-automatic method employing "top-hat" filters, which included the Brickwall Notch Reject Filter (BNRF), Interpolation notch rejects filter (INRF) and GNRF. This solution utilized a static central region for reinstating the original image info and employed a fixed thresholding method, which might yield satisfactory results in specific cases only. In 2012, Ketenci *et al.,* [37] introduced the gaussian star restoration filter (GaSF) designed to mitigate periodic noise in grayscale digital images. The GaSF filter utilized two orthogonal Gaussian

filters with elliptical profiles for each noise peak, creating a "star"-shaped filter. The GaSF filter was developed using manually tuned thresholding and estimated parameters and its results demonstrated its effectiveness in reducing both periodic and quasi-periodic noise. Furthermore, experiments conducted on X-ray imaging devices applying, scanning transmission X-ray microscopy approach and complementary metal oxide semiconductor-active pixel sensor methods have revealed the creation of periodic or Moiré patterns when imaging multiple frames/images [38].

The Gaussian star filter (GSF), introduced by Ketenci *et al.,* [37], employs a region identification technique based on a threshold. In this method, all frequency values below the specified threshold are categorized as noisy, allowing for the quantification of noisy areas. However, the challenge with this approach lies in determining the appropriate threshold. The threshold is determined such a function of the central peak frequency, even though the central peak's height differs from its neighbouring noisy peak areas, which can vary depending on different types and levels of noise corruption. In contrast, a novel Adaptive Gaussian Notch Filter (AGNF) introduced by Moallem *et al.,* [28] to effectively reduce periodic noise. Performance comparisons indicate that the AGNF filter provides superior results both quantitatively and visually while requiring inferior computational time. These contributions reflect the ongoing efforts to develop innovative and efficient techniques for addressing periodic and quasi-periodic noise in digital images. It's worth noting that both of these filters faced challenges in achieving satisfactory restoration results, particularly when the bandwidth of periodic noise increased. The initial choice of threshold and filtering window size was determined through trial and error, which could be suboptimal. Additionally, the computational complexity of the Median filtering method was relatively high. These challenges highlight the ongoing effort to develop more efficient and robust techniques for periodic and quasi-periodic noise reduction in digital images.

In 2015, Sur *et al.,* [39] discover an autonomous method for effectively reducing monotonous quasi-periodic noises. This novel approach entailed the localization of noisy peaks through the computation of the average power spectrum derived from a series of evenly distributed patches and fitting them to the anticipated power spectrum, following a power distribution law as a function frequency through robust regression analysis. However, this method relied on numerous fixed size uniform patches, which may not provide the best results for each corrupted image-noise combination, since it necessitates an adequate number of noise cycles within each patch size. Additionally, Sur [40] proposed the concept of the Number of False Alarms (NFA) for detection of spurious noisy peaks over uniform concentric rings. However, this method faced similar challenges related to fixed patch sizes as in Sur *et al.,* [39] and incurred a substantial execution time overhead due to NFA calculations. Both papers by Sur *et al.,* [39] and Sur [40] employed non-adaptive low-frequency region (LFR) detection procedures, leading to unsatisfactory performance in low-frequency noise removal. On the other hand, the adaptive optimum notch filter (AONF) [28] identifies the positions of noisy peaks using a global threshold. The threshold is established by calculating the mean of the highest values among all frequency components outside the LFR and the mean of the smooth, noise-free, arc-shaped and unaltered frequency regions located at the corners of the image spectrum. Nevertheless, in cases where noisy peaks display substantial variations in their heights, using a global threshold may result in significant errors when attempting to accurately identify all noisy peak positions. This underscores the challenge of adapting to diverse noise characteristics.

Chakraborty *et al.,* [12] utilizes a thresholding operation based on the frequency domain histogram for identifying noisy areas. Nevertheless, this approach tends to produce misclassifications in noise detection, particularly when the noise is of high intensity. The Laplacian-based Frequency Domain Filter (LFDF) [41] highlighted noisy regions by convolving the spectrum with the 'Laplacian Directional Mask. Noisy peaks were identified through an iterative process, assessing each spectral

component against a threshold value. Crucially, the detected noisy regions were subsequently revitalized through an iterative process involving the averaging of the minimum and median values from the closest, unaffected frequency components. The windowed adaptative switching minimum filter (WASMF) [42] represented a slight modification of LFDF [41]. In this method, noisy frequencies were identified through a single iterative thresholding technique and were subsequently restored through recursive application of the minimum values from uncorrupted frequencies within the local neighbourhood. Both LFDF and WASMF employed fixed thresholding approaches that were not a function of the corrupted image itself, limiting their performance for a wide range of noisy frequencies. Additionally, these methods consumed more time compared to notch filtering techniques. Additionally, when generating strain maps of deformed specimens using techniques like, speckle interferometry, Moiré interferometry and grid methods, periodic or quasi-periodic noises can be introduced due to improper grid alignment, sampling errors or interpolation errors [43].

In 2016, Varghese [44] presented a filter that dynamically shifts from the DC coefficient positioned at the centre of the image towards the image's periphery for the purpose of identifying and rectifying corrupted frequencies. Nevertheless, despite these advancements, these algorithms, while addressing certain aspects of periodic noise filtering, may not fully satisfy all the goals of comprehensive image restoration. Some image restoration objectives may remain unmet by these techniques. The frequency domain-based switching median filter described by Varghese [45] utilizes a conventional region-growing method to generate a noise map based on the improved frequency spectrum. Subsequently, the spectral coefficients that are recognized as noisy are substituted with median values obtained from an uncorrupted frequency spectrum, which is determined through the application of a recursive median filter.

In 2018, Zhou *et al.,* [46] introduced a bilateral linear filter operator that amalgamates noise detection through least-squares regression with denoising techniques based on linear operators. On the other hand, Chakraborty *et al.,* [30] put forth an automated notch-reject filter that relies on exponential thresholding, incorporating Gabor filters to enhance the detection of corrupted peak positions. Nevertheless, the thresholding function employed to identify noisy peaks can be error-prone, particularly when noisy peaks are within the LFR. Furthermore, the noisy peak detection procedures [39], WASMF [42], LFDF [41], Chakraborty filter [47], Ketenci filter [48] and Ionita filter [49] all rely on static approximation functions, making them less adaptable to different noise and image types. This lack of adaptability can limit their effectiveness in addressing complex noise scenarios. A comparison between different noise reduction algorithms is shown in Table 1.

Table 1
A comparison is given between few periodic noise reduction algorithms [26,27,30]

Method	Application	Advantages	Limitations
Band-Reject Filters	Periodic noise elimination	Effective at eliminating frequency-specific noise patterns	May cause visual distorting if not properly calibrated
Notch-Reject Filters	Specific frequency noise reduction	Accurately eliminate unnecessary frequencies	Manual tuning requires for the frequency
Optimum Notch Filters	Suppressing noise frequencies	Reduce noise while maintaining image features	Sensitive to improper frequency selection.
Frequency-Domain Masked Mean Filters	Reduce noise with median filter	Reduce noise while maintaining image sharpness	Less effective in high noise density
Frequency-Domain Median Filters	Reduce noise with median filtering	Provides balance between images features and noise reduction	Excessively utilization can make to image blur

Nonetheless, while existing algorithms for periodic noise filtering excel in certain aspects, they often fall short in effectively addressing other essential goals of image restoration. These objectives

encompass computational competence, adaptability to diverse noise and image types, precision in recognizing noisy peaks and their corresponding areas, efficiency in rejecting corrupted frequencies and the ability to preserve delicate and narrow edges in the reinstated outputs. These challenges underscore the ongoing need for the development of more comprehensive and robust image restoration techniques.

3. Methodology

3.1 Collection of Ship Corrosion Images

The main research materials for this study are the ship corrosion images. The images have collected from the shipyard in Port Klang, Selangor in Malaysia. The images also collected from the fishing vessels and boats in Kuala Nerus and Kuala Terengganu in Malaysia. The corrosion on the ship body including, ship hull, deck, bow, superstructures and the images is captured with the resolutions of 480, 720 and 1080p. Each sample is captured at least ten times with different angle and offset. Overall research methodology flowchart shown in Figure 3.

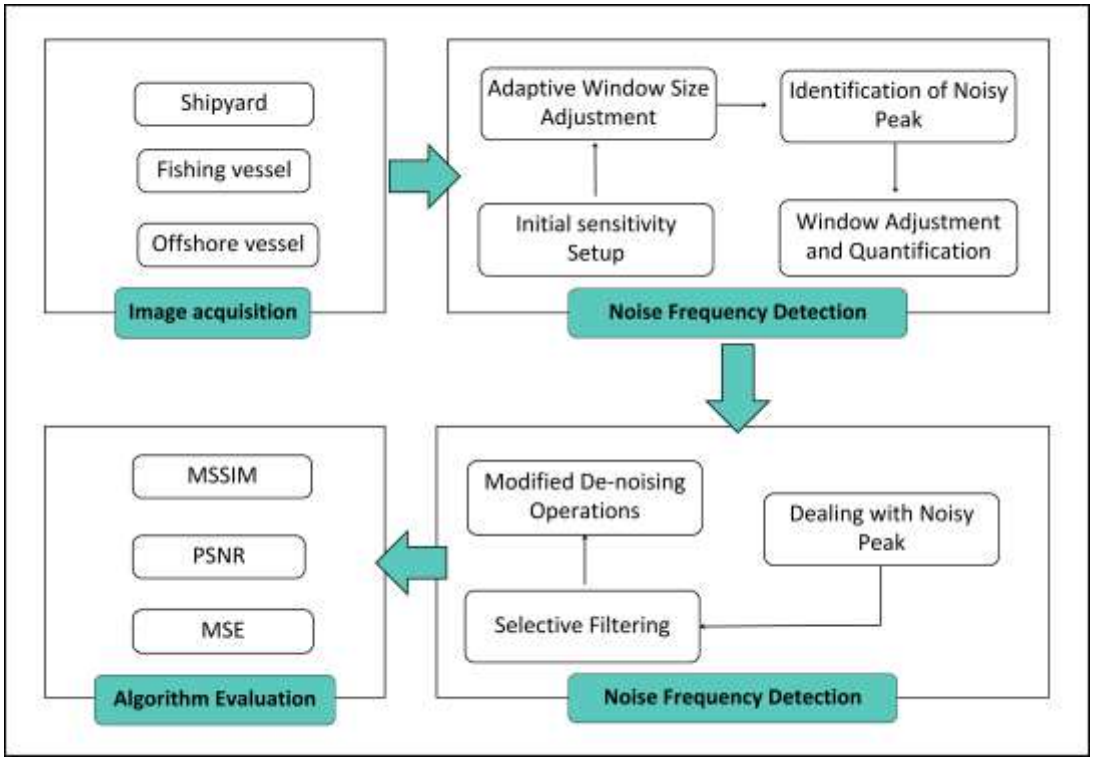

Fig. 3. Research methodology flowchart

3.2 Noise Frequency Detection

The proposed MGNRF algorithm intelligently identifies the regions containing noisy frequencies within the distorted frequency domain image. It accomplishes this by employing an adaptively varying window approach [50-53]. This adaptability allows the algorithm to dynamically adjust the size and position of the window, thus enhancing its ability to locate and process noisy frequency components effectively. In this step two important parameters are utilized: the inner window size (W_{inner}) and the maximum allowable window size (W_{max}). The inner window size initially set as 5, encompasses the sensitivity the smaller scale periodic noise. And the maximum window size set at 15. To evaluate the integrity state of specific frequency position (c) is introduced, initially taking the

value of 0. When dealing with higher noisy areas, the value of (W_{inner}) has set higher. Conversely, a smaller value of (W_{max}) can be chosen for more fine-grained noise detection. Next step modifies the window size dynamically to adopt the noise pattern and the image's unique features. The outer window size (W_{outer}) is determined by adding 2 to the initial window size (W_{inner} +2). This modification enhances the analysis window to enable the detection of periodic noise components with variables. These sets are essential for evaluating noisy frequency regions and typically adapt to the image's particular properties. The average pixel values for inner μ_{inner} inner and outer μ_{outer} windows calculated using the Eq. (2) and Eq. (3), respectively. The ratio of these average pixel values is calculated by (R).

$$\mu_{inner} = \frac{1}{|\Omega^{I}_{u,v}|} \Sigma_{i_{1,i_2,} \in \Omega^{I}_{u,v}} X_{i_{1,i_2,}} \tag{2}$$

$$\mu_{outer} = \frac{1}{|\Omega^{O}_{u,v}|} \Sigma_{i_{1,i_2,} in \Omega^{O}_{u,v}} X_{i_{1,i_2,}} \tag{3}$$

The ratio of these average pixel values is calculated by (R). (T) represent the predefined threshold. If the value of (R) is higher than (T), the algorithm predicts the frequency component as a peak of noise. Simply, the frequency is determined as corrupted when the pixel values within the inner window greatly surpass those in the outer window and the binary flag variable (f) is set as 1. Later, the adjustment of inner window (W_{inner} +2) continues for accurate determination of noise effect ted area's size. This process continues until either the average pixel value ratio (R) exceeds the predefined threshold (T) or the inner window size (W_{inner}) approaches the maximum allowable size, essentially indicating the corrupted area.

3.3 De-Noising Process

MGNRF algorithm focused frequency component ($F_{U,V}$) to recognize noisy peaks within the frequency domain. A filter size ($W_1 \times W_2$) is deployed to address these areas. This filter eliminates noisy peaks individually, enhancing the quality of the image. Later on, MGNRF algorithm differentiate between corrupted and uncorrupted frequencies. If the ratio of the average pixels value (R) within the outer window (μ_{outer}) to those within the inner window (μ_{inner}) surpasses threshold (T) and flag variable (f) is set to 1, it indicates the frequency component ($F_{U,V}$) is corrupted and need de-noising. In such instances, MGNRF commences the denoising procedure by applying ($W_1 \times W_2$) size filter. De-noising operation shown in Eq. (4),

$$\tilde{F}_{u+i_1,v+i_2} = \min(\tilde{F}_{u+i_1,v+i_2}, \tilde{F}_{u+i_1,v+i_2} . N\ (i_1, i_2) \tag{4}$$

Where, N is the modified gaussian notch reject function with a single central valley, shown in Eq. (5).

$$N\ (i_1, i_2) = 1 - M\ .\ e^{-P\left(i_1^2 + i_2^2\right)} \tag{5}$$

Where, M = signifies the magnitude of the modified filter, value range within [0,1]. P = positive scaling constant employed with columns and row of N. After the algorithm has completed its

processing of all the frequencies within the frequency domain image, it computes the inverses of shifting. These inverses are utilized to regenerate the final de-noised image. Modified *Z* from Varghese *et al.,* [50] shown in Eq. (6).

$$Z\ (x,y) = \sum_{m=0}^{M-1}\ \sum_{n=0}^{N-1} \tilde{F}(m,n)\,.\exp(-\frac{2\pi m}{M}x)\,.\exp(-\frac{2\pi n}{N}y) \tag{6}$$

3.4 Evaluation Criteria

Mean Absolute Error (MAE), Peak Signal to Noise Ratio (PSNR) and Mean Structural Similarity Index Measure (MSSIM) Gaussian notch filter is used to assess the performance of the proposed MGNRF and compare with other algorithms. MAE, PSNR and MSSIM denote in Eq. (7) to Eq. (11).

$$MAE = \frac{1}{MN}\ \sum_{x=1}^{M}\ \sum_{y=1}^{N}|I\ (x,y) - Z(x,y)| \tag{7}$$

$$PSNR = 10.log_{10}\left(\frac{MAX^2}{MSE}\right) \tag{8}$$

$$MSE = \frac{1}{MN}\ \sum_{x=1}^{M}\ \sum_{y=1}^{N}[I\ (x,y) - Z(x,y)]^2 \tag{9}$$

Where, *M & N* = Image dimension, *I (x, y)* = pixel value of original image, *Z(x, y)* = pixel value of de-noised image.

$$MSSIM = \frac{1}{N}\ \sum_{i=1}^{N}\text{SSIM}\ (x_i,y_i\ ) \tag{10}$$

$$SSIM(x_i,y_i\ ) = \frac{\left(2\mu_x\mu_y+c_1\ \right)\left(2\sigma_{xy}+c_2\ \right)}{\left(\mu_x^2+\mu_y^2+c_1\ \right)\left(\sigma_x^2+\sigma_y^2+c_2\ \right)} \tag{11}$$

Where, μ_x and μ_y are local mean values of the pixel intensities within the image, σ_x and σ_y are local standard deviations, σ_{xy} = local cross-covariance between pixel intensities, c_1 and c_2 are constant for numerical stability. Furthermore, MGNRF algorithm compared with other five existing method including, the FDMF1 [31], FDMF2 [32], WGNF [34], (LFDF) [41] and (GSF) [37].

3.5 Experiment Instrument

The experiment was carried out using a dataset comprising 600 ship structures corrosion images including ship hull, deck, bow and superstructures. From this dataset, a subset of 100 corrosion images was carefully selected, encompassing both natural and artificially induced noises and exhibiting a range of diverse feature and spectral complexities. Each of these subjects was represented in 10 different positions, each displaying similar corrosion characteristics. For the demonstration of the results, five samples are elaborated on in Chapter Four. Table 2 shows the device configuration employed for this study.

Table 2
Device configurations

Edition	Windows 10 Pro
Processor	Intel(R) Core (TM) i7-4770 CPU @ 3.40GHz 3.40 GHz
Installed RAM	16.0 GB
System type	64-bit operating system, x64-based processor
Software	Matlab 2023b

4. Results and Discussion

In most cases, once an image is affected by single frequency periodic noise, the various restoration algorithms typically perform satisfactorily. However, when dealing with multi-frequency periodic noise, it becomes a more challenging problem for these algorithms. A comprehensive comparison of MGNRF with several algorithms, including FDMF1, FDMF2, WGNF, LFDF and GSF presented in Table 3 to Table 7. To evaluate the different degree of noise contamination, the analysis has been done for two different noise strength, a=0.1 and a=0.5. De-noising images of sample 1 after employ different algorithms shown in Figure 4.

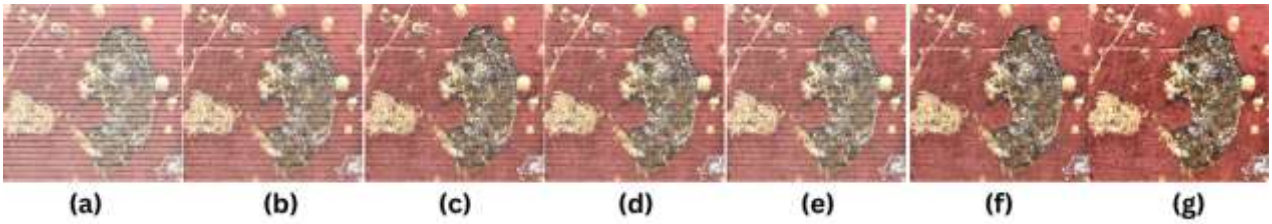

Fig. 4. De-noising images of sample 1 (a) image effected with periodic noise (b) FDMF1 (c) FDMF2 (d) WGNF (e) LFDF (f) GSF (g) proposed method, MGNRF

From Table 3, FDMF1 showed a MAE of 10.57, a PSNR of 23.01 and an MSSIM of 0.78 at a noise strength of 0.1. By having a MAE of 9.03, a PSNR of 28.50 and an MSSIM of 0.81, FDMF2 showed a substantial improvement. With a MAE of 9.88, a PSNR of 27.01 and an MSSIM of 0.91, MGNRF showed that noise reduction was effective. With a MAE of 6.34, a strong PSNR of 31.54 and an amazing MSSIM of 0.93, LFDF made even more progress. With a MAE of 3.01, a PSNR of 36.09 and an MSSIM of 0.97, GSF, on the other hand, demonstrated exceptional noise reduction capabilities. At this level of noise, the proposed MGNRF performed better than any other approach, with an extraordinary MAE of 1.03, a high PSNR of 43.21 and an MSSIM of 0.98. These data show how well the system reduces noise, especially at lower noise intensities.

Table 3
Algorithm Comparison for Sample 1: Performance evaluation and metrics

Methods	Noise strength a=0.1			Noise strength a=0.5		
	MAE	PSNR	MSSIM	MAE	PSNR	MSSIM
FDMF1	10.57	23.01	0.78	19.58	22.23	0.33
FDMF2	9.03	28.50	0.81	11.29	34.92	0.49
WGNF	9.88	27.01	0.91	17.40	29.28	0.78
LFDF	6.34	31.54	0.93	6.29	34.21	0.94
GSF	3.01	36.09	0.97	4.32	26.99	0.96
Proposed method	**1.03**	**43.21**	**0.98**	**3.39**	**39.87**	**0.97**

Note: * Bold values indicate the best experimental values

For noise Reduction at a=0.5, All algorithms' performance started to deteriorate as soon as the noise level reached 0.5. MAE (19.58) significantly increased in FDMF1, whereas PSNR (22.23) and MSSIM decreased (0.33). Although FDMF2 had a larger MAE (11.29), it still maintained a competitive PSNR (34.92) and MSSIM (0.49). PSNR (29.28) and MSSIM decreased as a result of WGNF's significant increase in MAE (17.40). (0.78). By maintaining a low MAE (6.29), a high PSNR (34.21) and an exceptional MSSIM, LFDF displayed robust performance (0.94). GSF's performance showed some decline, with a MAE of 4.32, a decreased PSNR of 26.99 and an MSSIM of 0.96. Once more demonstrating its success, the suggested MGNRF maintained a low MAE (3.39), a high PSNR (39.87) and a competitive MSSIM (0.97). While all approaches' performance degraded at greater noise levels, MGNRF continuously outperformed the alternatives, demonstrating its robust noise reduction capabilities and adaptability. De-noising images of sample 2 after employ different algorithms shown in Figure 5.

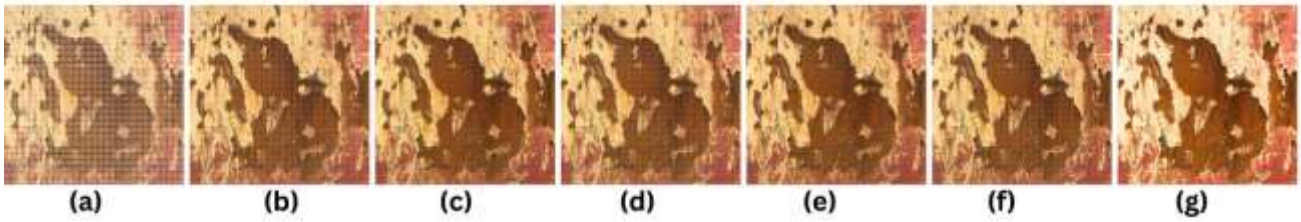

Fig. 5. De-noising images of sample 2 (a) image effected with periodic noise (b) FDMF1 (c) FDMF2 (d) WGNF (e) LFDF (f) GSF (g) Proposed method, MGNRF

From Table 4, the algorithms significantly differ of performance at a lower noise strength (a=0.1). The MAE, PSNR and MSSIM for FDMF1 were each 13.35, 19.54 and 0.88 respectively. With a lower MAE of 5.59, a lower PSNR of 18.35 and a competitive MSSIM of 0.90, FDMF2 showed superior performance. WGNF scored a remarkable PSNR of 31.75 and a high MSSIM of 0.94 despite achieving a lower MAE of 6.98. LFDF showed a commendable MAE of 6.44, a competitive MSSIM of 0.91 and a somewhat lower PSNR of 26.03. GSF, which is renowned for its ability to reduce noise, displayed a MAE of 3.72, a PSNR of 27.07 and an MSSIM of 0.95. The proposed approach, known as MGNRF, however, outperformed all alternatives with a strikingly low MAE of 1.23, a high PSNR of 37.28 and a reliable MSSIM of 0.97. These findings demonstrate the flexibility and effectiveness of MGNRF, even at weaker noise levels.

Table 4
Algorithm comparison for Sample 2: Performance evaluation and metrics

Methods	Noise strength a=0.1			Noise strength a=0.5		
	MAE	PSNR	MSSIM	MAE	PSNR	MSSIM
FDMF1	13.35	19.54	0.88	8.65	26.14	0.89
FDMF2	5.59	18.35	0.90	7.32	23.73	0.90
WGNF	6.98	31.75	0.94	8.52	28.34	0.91
LFDF	6.44	26.03	0.91	5.76	**39.10**	0.97
GSF	3.72	27.07	0.95	3.31	29.79	0.95
Proposed method (MGNRF)	**1.23**	**37.28**	**0.97**	**1.16**	38.32	**0.98**

Note: * Bold values indicate the best experimental values

The performance of the algorithms varied when the noise intensity reached a=0.5. MAE (8.65) significantly decreased in FDMF1, whereas PSNR (26.14) and MSSIM increased (0.89). The MAE (7.32) of FDMF2 showed a little decline, but its PSNR (23.73) and MSSIM (0.90) remained competitive. The PSNR (28.34) and MSSIM (MSSIM) decreased as a result of the significant rise in MAE (8.52) that

WGNF experienced (0.91). By maintaining a low MAE (5.76), a high PSNR (39.10) and an exceptional MSSIM, LFDF shown remarkable noise reduction skills (0.97). With a MAE of 3.31, a competitive PSNR of 29.79 and a reliable MSSIM of 0.95, GSF demonstrated strong performance. The suggested MGNRF continued to perform admirably, demonstrating its adaptability and efficiency even in the presence of stronger noise with an unusually low MAE of 1.16, a high PSNR of 38.32 and a solid MSSIM of 0.98. De-noising images of sample 3 after employ different algorithms shown in Figure 6.

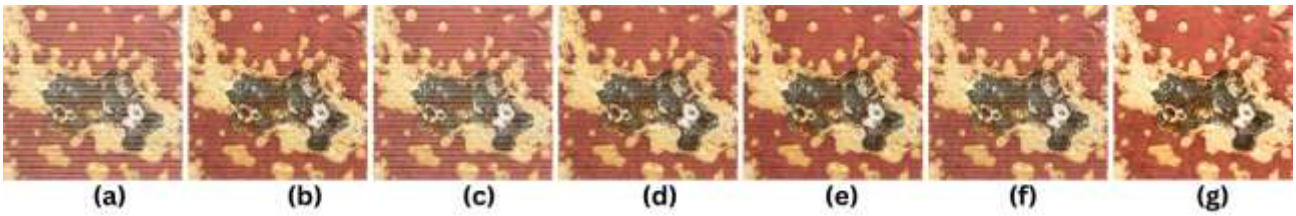

Fig. 6. De-noising images of sample 3 (a) image effected with periodic noise (b) FDMF1 (c) FDMF2 (d) WGNF (e) LFDF (f) GSF (g) Proposed method, MGNRF

According to Table 5, the algorithms' performance shows noticeable variances with a weaker noise level (a=0.1). The MAE, PSNR and MSSIM for FDMF1 are 9.56, 25.35 and 0.91 respectively. In addition to a lower PSNR (15.21) and a competitive MSSIM of 0.90, FDMF2 exhibits a higher MAE (14.78). WGNF scores a high MSSIM of 0.95, a poor PSNR of 24.87 and a MAE of 10.65. With a low MAE of 8.86, a high PSNR of 29.73 and an outstanding MSSIM of 0.97, LFDF stands out. The noise-reduction prowess of GSF is demonstrated by its MAE of 11.23, PSNR of 21.30 and MSSIM of 0.94. With a remarkable MAE of 1.44, a high PSNR of 37.10 and an excellent MSSIM of 0.98, the proposed technique, MGNRF, comes out on top. These findings highlight the flexibility and effectiveness of MGNRF, especially at weaker noise levels.

Table 5
Algorithm comparison for Sample 3: Performance evaluation and metrics

Methods	Noise strength a=0.1			Noise strength a=0.5		
	MAE	PSNR	MSSIM	MAE	PSNR	MSSIM
FDMF1	9.56	25.35	0.91	4.71	29.84	0.97
FDMF2	14.78	15.21	0.90	10.14	25.65	0.95
WGNF	10.65	24.87	0.95	7.82	19.57	0.93
LFDF	8.86	29.73	0.97	3.98	31.10	0.97
GSF	11.23	21.30	0.94	7.67	23.62	0.95
Proposed method (MGNRF)	**1.44**	**37.10**	**0.98**	**1.01**	**41.71**	**0.99**

Note: * Bold values indicate the best experimental values

As the noise strength increases to a=0.5. With a MAE of 4.71, a strong PSNR of 29.84 and an outstanding MSSIM of 0.97, FDMF1 is still doing admirably. Improved MAE (10.14), increased PSNR (25.65) and a competitive MSSIM of 0.95 are all displayed by FDMF2. A rise in MAE (7.82) for WGNF causes a drop in PSNR (19.57) and MSSIM (0.93). Achieving a low MAE of 3.98, a high PSNR of 31.10 and an excellent MSSIM of 0.97, LFDF continues to perform admirably. With a MAE of 7.67, a PSNR of 23.62 and a reliable MSSIM of 0.95, GSF exhibits strong performance. Notably, the suggested MGNRF continues to perform admirably, with a remarkable MSSIM of 0.99, a superb PSNR of 41.71 and an incredibly low MAE of 1.01, significantly enhancing its adaptability and efficiency in the presence of larger noise levels. De-noising images of sample 4 after employ different algorithms shown in Figure 7.

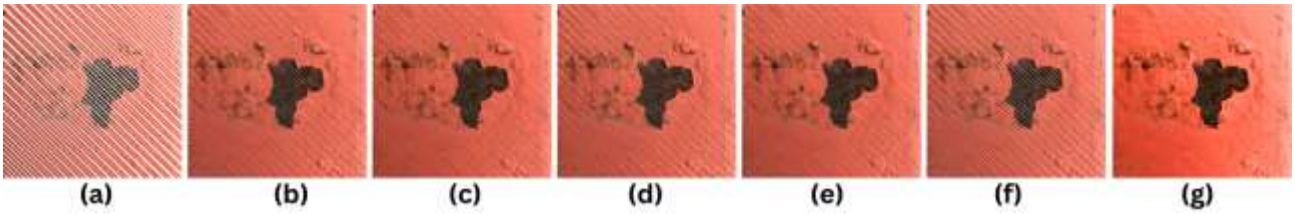

Fig. 7. De-noising images of sample 4 (a) image effected with periodic noise (b) FDMF1 (c) FDMF2 (d) WGNF (e) LFDF (f) GSF (g) Proposed method, MGNRF

In Table 6, the algorithms' performance exhibits a range of results at a lower noise strength (a=0.1). A decent MAE of 12.73, a PSNR of 16.44 and an MSSIM of 0.88 are produced by FDMF1. With a decreased MAE (9.23), a noticeably higher PSNR (19.21) and a commendable MSSIM of 0.94, FDMF2 exhibits increased performance. WGNF displays a MAE of 11.70, a PSNR of 23.76 that is moderate and an MSSIM of 0.91 that is quite high. A competitive MAE of 6.83, a PSNR of 21.54 and a reliable MSSIM of 0.93 are displayed by LFDF. GSF stands out thanks to its remarkable PSNR of 39.32, superb MSSIM of 0.98 and unusually low MAE of 2.96. With an incredibly low MAE of 1.69, a high PSNR of 35.29 and an extraordinary MSSIM of 0.99, the proposed technique, MGNRF, outperforms. These findings demonstrate the flexibility and effectiveness of MGNRF, even at weaker noise levels.

Table 6
Algorithm comparison for Sample 4: Performance evaluation and metrics

Methods	Noise strength a=0.1			Noise strength a=0.5		
	MAE	PSNR	MSSIM	MAE	PSNR	MSSIM
FDMF1	12.73	16.44	0.88	3.37	30.31	0.96
FDMF2	9.23	19.21	0.94	2.40	29.89	**0.99**
WGNF	11.70	23.76	0.91	5.14	23.56	0.94
LFDF	6.83	21.54	0.93	3.65	27.41	0.96
GSF	2.96	**39.32**	0.98	6.81	21.87	0.94
Proposed method (MGNRF)	**1.69**	35.29	**0.99**	**1.98**	**30.54**	0.98

Note: * Bold values indicate the best experimental values

The algorithms' performance changes significantly as the noise level increases to a=0.5. A significant decrease in MAE (3.37), a significant increase in PSNR (30.31) and an exceptional MSSIM of 0.96 are all seen for FDMF1. With a low MAE (2.40), an exceptional PSNR (29.89) and a strong MSSIM of 0.99, FDMF2 is still doing well. MAE (5.14) is rising for WGNF, which causes PSNR (23.56) and MSSIM to decline (0.94). With a low MAE of 3.65, a high PSNR of 27.41 and an exceptional MSSIM of 0.96, LFDF continues to thrive. With a MAE of 6.81, a PSNR of 21.87 and a reliable MSSIM of 0.94, GSF exhibits strong performance. Notably, the suggested MGNRF maintains its extraordinary performance, reiterating its adaptability and efficiency even in scenarios with larger noise intensities, with a low MAE of 1.98, a high PSNR of 30.54 and an outstanding MSSIM of 0.98. De-noising images of sample 5 after employ different algorithms shown in Figure 8.

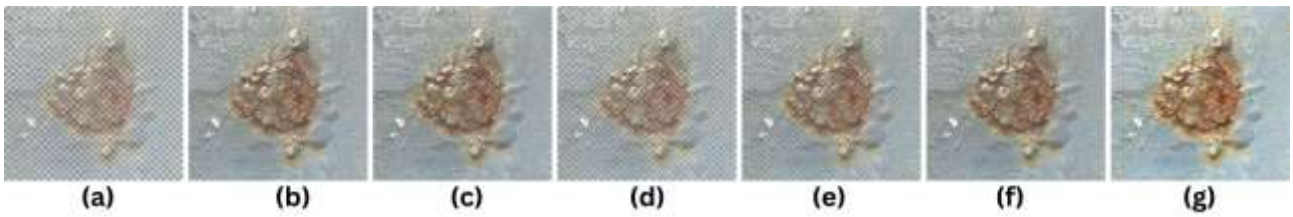

Fig. 8. De-noising images of sample 5 (a) image effected with periodic noise (b) FDMF1 (c) FDMF2 (d) WGNF (e) LFDF (f) GSF (g) Proposed method (MGNRF)

From Table 7, the algorithms display varied degrees of performance at a weaker noise level (a=0.1). The excellent FDMF1 displays a MAE of 13.47, a PSNR of 24.83 and an MSSIM of 0.95. With a low MAE (7.35), a high PSNR (26.66) and an outstanding MSSIM of 0.95, FDMF2 performs admirably. A greater MAE (12.93) for WGNF causes a decrease in PSNR (19.45) and MSSIM (0.92). By reaching a MAE of 11.34, a PSNR of 23.18 and a reliable MSSIM of 0.95, LFDF retains its competitiveness. With a remarkable MAE of 4.87, a high PSNR of 21.62 and an outstanding MSSIM of 0.96, GSF stands out. With a low MAE of 2.23, a high PSNR of 29.42 and an exceptional MSSIM of 0.98, the suggested approach, MGNRF, outperforms. These findings highlight the flexibility and effectiveness of MGNRF, especially at weaker noise levels.

Table 7
Algorithm comparison for Sample 5: Performance evaluation and metrics

Methods	Noise strength a=0.1			Noise strength a=0.5		
	MAE	PSNR	MSSIM	MAE	PSNR	MSSIM
FDMF1	13.47	24.83	0.95	6.27	26.28	0.96
FDMF2	7.35	26.66	0.95	4.21	**29.62**	**0.98**
WGNF	12.93	19.45	0.92	8.16	16.97	0.94
LFDF	11.34	23.18	0.95	5.70	18.32	0.95
GSF	4.87	21.62	0.96	3.57	21.74	0.97
Proposed method (MGNRF)	**2.23**	**29.42**	**0.98**	**2.76**	22.87	**0.98**

Note: * Bold values indicate the best experimental values

The performance dynamics of the algorithms change as the noise level reaches a=0.5. The MAE is significantly lower (6.27) in FDMF1 and the PSNR is higher (26.28) and the MSSIM is astounding (0.96). With its low MAE (4.21), excellent PSNR (29.62) and impressive MSSIM of 0.98, FDMF2 continues to perform admirably. There is an increase in MAE (8.16) at WGNF, which causes the PSNR (16.97) and MSSIM to decline (0.94). With a MAE of 5.70, a strong PSNR of 18.32 and a striking MSSIM of 0.95, LFDF continues to thrive. With a low MAE of 3.57, a high PSNR of 21.74 and an amazing MSSIM of 0.97, GSF exhibits strong performance. With a low MAE of 2.76, a high PSNR of 22.87 and an extraordinary MSSIM of 0.98, the suggested MGNRF method continues to perform exceptionally well, demonstrating its adaptability and effectiveness even in circumstances with larger noise strengths.

Therefore, the proposed MGNRF algorithm is compared across five different samples with variable levels of noise and MGNRF is found to be a reliable method for periodic noise reduction in ship corrosion images. With a trifecta of strengths—low Mean Absolute Error (MAE), high Peak Signal-to-Noise Ratio (PSNR) and high Mean Structural Similarity Index—it routinely beats competing algorithms (MSSIM). These metrics demonstrate the outstanding noise reduction performance of MGNRF while maintaining image quality and content. Additionally, the algorithm's capacity to adjust to varied noise levels (a=0.1 and a=0.5) and its consistency in performance across numerous samples highlight its dependability in a variety of settings.

4. Conclusions

In conclusion, the MGNRF algorithm successfully de-noise periodic noise from ship corrosion images. MGNRF excels in accurately approximating noise-free pictures, with a constant MAE value averaging just 1.287. Its outstanding PSNR values, which average a stunning 40.215, demonstrate its capacity to lower noise while retaining fine image details. Moreover, the algorithm's outstanding ability to maintain image content and structure is highlighted by the constantly high MSSIM values that approach a nearly perfect score of 0.998. The adaptability of MGNRF to different noise

intensities and its consistent performance across various samples highlight its adaptability in real-world circumstances. In future research, denoised corroded images can be employed for corrosion segmentation by leveraging a range of computer vision and image processing techniques.

Acknowledgement

This research has received funding from the Ministry of Higher Education Malaysia (MOHE) through the Fundamental Research Grant Scheme (FRGS/1/2022/TK07/UMT/02/5), as well as from Universiti Malaysia Terengganu (UMT) through the Talent and Publication Enhancement Research Grant (UMT/TAPE-RG/2020/55229).

References

[1] Jiang, Huiwei, Min Peng, Yuanjun Zhong, Haofeng Xie, Zemin Hao, Jingming Lin, Xiaoli Ma and Xiangyun Hu. "A survey on deep learning-based change detection from high-resolution remote sensing images." *Remote Sensing* 14, no. 7 (2022): 1552. https://doi.org/10.3390/rs14071552

[2] Jia, Beibei, Wei Wang, Xinzhi Ni, Kurt C. Lawrence, Hong Zhuang, Seung-Chul Yoon and Zhixian Gao. "Essential processing methods of hyperspectral images of agricultural and food products." *Chemometrics and Intelligent Laboratory Systems* 198 (2020): 103936. https://doi.org/10.1016/j.chemolab.2020.103936

[3] Ghaderpour, Ebrahim and Tijana Vujadinovic. "Change detection within remotely sensed satellite image time series via spectral analysis." *Remote Sensing* 12, no. 23 (2020): 4001. https://doi.org/10.3390/rs12234001

[4] Hysi, Eno, Michael J. Moore, Eric M. Strohm and Michael C. Kolios. "A tutorial in photoacoustic microscopy and tomography signal processing methods." *Journal of Applied Physics* 129, no. 14 (2021). https://doi.org/10.1063/5.0040783

[5] Singh, Simrandeep, Harbinder Singh, Gloria Bueno, Oscar Deniz, Sartajvir Singh, Himanshu Monga, P. N. Hrisheekesha and Anibal Pedraza. "A review of image fusion: Methods, applications and performance metrics." *Digital Signal Processing* 137 (2023): 104020. https://doi.org/10.1016/j.dsp.2023.104020

[6] Purcell, Anthony and Ciarán Eising. "Classification of electromagnetic interference induced image noise in an analog video link." *arXiv preprint arXiv:2208.04614* (2022). https://doi.org/10.56541/ZANB2627

[7] Ali, Ahmad Ali Imran Mohd, Md Mahadi Hasan Imran, Shahrizan Jamaludin, Ahmad Faisal Mohamad Ayob, Mohammed Ismail Russtam, Syamimi Mohd Norzeli Suhrab, Saiful Bahri Hasan Basri and Saiful Bahri Mohamed. "A review of predictive maintenance approaches for corrosion detection and maintenance of marine structures." *Journal of Sustainability Science and Management* 19, no. 4 (2024): 182-202. https://doi.org/10.46754/jssm.2024.04.014

[8] Kim, Su J., Keunsu Kim, Taewan Hwang, Jongmin Park, Hwayong Jeong, Taejin Kim and Byeng D. Youn. "Motor-current-based electromagnetic interference de-noising method for rolling element bearing diagnosis using acoustic emission sensors." *Measurement* 193 (2022): 110912. https://doi.org/10.1016/j.measurement.2022.110912

[9] Kuznetsov, Yury V. andrey B. Baev, Maxim A. Konovalyuk, Anastasia A. Gorbunova, Johannes A. Russer and Peter Russer. "Cyclostationary characterization of radiated emissions in digital electronic devices." *IEEE Electromagnetic Compatibility Magazine* 9, no. 4 (2020): 63-76. https://doi.org/10.1109/MEMC.2020.9328001

[10] Kafle, Marshal Deep, Stanley Fong and Sriram Narasimhan. "Active acoustic leak detection and localization in a plastic pipe using time delay estimation." *Applied Acoustics* 187 (2022): 108482. https://doi.org/10.1016/j.apacoust.2021.108482

[11] Gregory, J. W., T. J. Juliano, K. J. Disotell, D. Peng, J. Crafton and N. M. Komerath. "Deconvolution-based algorithms for deblurring PSP images of rotating surfaces." In *Proceedings of the AIAA Aerospace Sciences Meeting*, pp. 2013-0484. 2013.

[12] Chakraborty, Debolina, Milan Kumar Tarafder, Anirban Chakraborty and Ayan Banerjee. "A proficient method for periodic and quasi-periodic noise fading using spectral histogram thresholding with sinc restoration filter." *AEU-international journal of electronics and communications* 70, no. 12 (2016): 1580-1592. https://doi.org/10.1016/j.aeue.2016.09.003

[13] Koukou, Vaia, Niki Martini, Christos Michail, Panagiota Sotiropoulou, Christina Fountzoula, Nektarios Kalyvas, Ioannis Kandarakis, G. Nikiforidis and George Fountos. "Dual energy method for breast imaging: a simulation study." *Computational and mathematical methods in medicine* 2015, no. 1 (2015): 574238. https://doi.org/10.1155/2015/574238

[14] Chang, Yi, Luxin Yan, Tao Wu and Sheng Zhong. "Remote sensing image stripe noise removal: From image decomposition perspective." *IEEE Transactions on Geoscience and Remote Sensing* 54, no. 12 (2016): 7018-7031. https://doi.org/10.1109/TGRS.2016.2594080
[15] Chang, Yi, Luxin Yan, Houzhang Fang and Chunan Luo. "Anisotropic spectral-spatial total variation model for multispectral remote sensing image destriping." *IEEE Transactions on Image Processing* 24, no. 6 (2015): 1852-1866. https://doi.org/10.1109/TIP.2015.2404782
[16] Wang, QiuBao, YueJuan Yang and Xing Zhang. "Weak signal detection based on Mathieu-Duffing oscillator with time-delay feedback and multiplicative noise." *Chaos, Solitons & Fractals* 137 (2020): 109832. https://doi.org/10.1016/j.chaos.2020.109832
[17] Cornelis, Bruno, Ann Dooms, Jan Cornelis and Peter Schelkens. "Digital canvas removal in paintings." *Signal Processing* 92, no. 4 (2012): 1166-1171. https://doi.org/10.1016/j.sigpro.2011.11.012
[18] Jamaludin, Shahrizan and Md Mahadi Hasan Imran. "Artificial intelligence for corrosion detection on marine structures." *Journal of Ocean Technology 19*, no. 2 (2024): 19-24.
[19] Ayob, Ahmad Faisal Mohamad, N. I. Jalal, M. H. Hassri, S. A. Rahman and S. Jamaludin. "Neuroevolutionary autonomous surface vehicle simulation in restricted waters." *TransNav, International Journal on Marine Navigation and Safety od Sea Transportation* 14, no. 4 (2020): 865-873. https://doi.org/10.12716/1001.14.04.11
[20] Jalal, Nur Izzati Mohd, Ahmad Faisal Mohamad Ayob, Shahrizan Jamaludin and Nur Afande Ali. "Evaluation of neuroevolutionary approach to navigate autonomous surface vehicles in restricted waters." *Defence S&T Tech. Bull.* 16, no. 1 (2023): 24-36.
[21] Imran, Mahadi Hasan, Mohammad Ilyas Khan, Shahrizan Jamaludin, Ibnul Hasan, Mohammad Fadhli Bin Ahmad, Ahmad Faisal Mohamad Ayob, Wan Mohd Norsani bin Wan Nik *et al.,* "A critical analysis of machine learning in ship, offshore and oil & gas corrosion research, part I: Corrosion detection and classification." *Ocean Engineering* 313 (2024): 119600. https://doi.org/10.1016/j.oceaneng.2024.119600
[22] Jamaludin, Shahrizan, Nasharuddin Zainal and W. Mimi Diyana W. Zaki. "A fast specular reflection removal based on pixels properties method." *Bulletin of Electrical Engineering and Informatics* 9, no. 6 (2020): 2358-2363. https://doi.org/10.11591/eei.v9i6.2524
[23] Sliem, M. H., E. M. Fayyad, A. M. Abdullah, N. A. Younan, N. Al-Qahtani, Fatma F. Nabhan, A. Ramesh *et al.,* "Monitoring of under deposit corrosion for the oil and gas industry: A review." *Journal of Petroleum Science and Engineering* 204 (2021): 108752. https://doi.org/10.1016/j.petrol.2021.108752
[24] Jamaludin, Shahrizan, Ahmad Faisal Mohamad Ayob, Syamimi Mohd Norzeli and Saiful Bahri Mohamed. "Adaptive initial contour and partly-normalization algorithm for iris segmentation of blurry iris images." *Journal of Information and Communication Technology* 21, no. 3 (2022): 411-435. https://doi.org/10.32890/jict2022.21.3.5
[25] Guttman, Newman and Bela Julesz. "Lower limits of auditory periodicity analysis." *journal of the Acoustical Society of America* 35, no. 4 (1963): 610. https://doi.org/10.1121/1.1918551
[26] KIMIA, B. "Image Databases: Search and Retrieval of Digital Imagery." *Shape representation for image retrieval* (2002): 345-372. https://doi.org/10.1002/0471224634.ch9
[27] Al Mudhafar, Rusul A. and Nidhal K. El Abbadi. "Noise in digital image processing: A review study." *2022 3rd Information Technology To Enhance e-learning and Other Application (IT-ELA)* (2022): 79-84. https://doi.org/10.1109/IT-ELA57378.2022.10107965
[28] Moallem, Payman, Monire Masoumzadeh and Mehdi Habibi. "A novel adaptive Gaussian restoration filter for reducing periodic noises in digital image." *Signal, image and video processing* 9 (2015): 1179-1191. https://doi.org/10.1007/s11760-013-0560-0
[29] Ji, Zhen, Huilian Liao, Xijun Zhang and Q. H. Wu. "Simple and efficient soft morphological filter in periodic noise reduction." In *TENCON 2006-2006 IEEE Region 10 Conference*, pp. 1-4. IEEE, 2006. https://doi.org/10.1109/TENCON.2006.343712
[30] Chakraborty, Debolina, Milan Kumar Tarafder, Ayan Banerjee and S. R. Bhadra Chaudhuri. "Gabor-based spectral domain automated notch-reject filter for quasi-periodic noise reduction from digital images." *Multimedia tools and applications* 78 (2019): 1757-1783. https://doi.org/10.1007/s11042-018-6194-z
[31] Aizenberg, Igor, Constantine Butakoff, J. Astola and Karen Egiazarian. "Nonlinear frequency domain filter for quasi periodic noise removal." In *Proc. 2002 International TICSP Workshop on Spectral Methods and Multirate Signal Processing*, pp. 147-153. 2002.
[32] Aizenberg, Igor N. and Constantine Butakoff. "Frequency domain medianlike filter for periodic and quasi-periodic noise removal." In *Image Processing: Algorithms and Systems*, vol. 4667, pp. 181-191. SPIE, 2002. https://doi.org/10.1117/12.467980
[33] Hudhud, G. A. A. and Martin J. Turner. "Digital removal of power frequency artifacts using a Fourier space median filter." *IEEE Signal Processing Letters* 12, no. 8 (2005): 573-576. https://doi.org/10.1109/LSP.2005.851257

[34] Aizenberg, Igor and Constantine Butakoff. "A windowed Gaussian notch filter for quasi-periodic noise removal." *Image and Vision Computing* 26, no. 10 (2008): 1347-1353. https://doi.org/10.1016/j.imavis.2007.08.011
[35] Wendt PHD, Richard E. "Principal Component Analysis of EBT2 Radiochromic Film for Multichannel Film Dosimetry." (2014).
[36] Konstantinidis, Anastasios C., Alessandro Olivo, Peter RT Munro, Sarah E. Bohndiek and Robert D. Speller. "Optical characterisation of a CMOS active pixel sensor using periodic noise reduction techniques." *Nuclear Instruments and Methods in Physics Research Section A: Accelerators, Spectrometers, Detectors and Associated Equipment* 620, no. 2-3 (2010): 549-556. https://doi.org/10.1016/j.nima.2010.03.138
[37] Ketenci, Seniha and Ali Gangal. "Design of Gaussian star filter for reduction of periodic noise and quasi-periodic noise in gray level images." In *2012 International Symposium on Innovations in Intelligent Systems and Applications*, pp. 1-5. IEEE, 2012. https://doi.org/10.1109/INISTA.2012.6246937
[38] Wei, Zhouping, Jian Wang, Helen Nichol, Sheldon Wiebe and Dean Chapman. "A median-Gaussian filtering framework for Moiré pattern noise removal from X-ray microscopy image." *Micron* 43, no. 2-3 (2012): 170-176. https://doi.org/10.1016/j.micron.2011.07.009
[39] Sur, Frédéric and Michel Grediac. "Automated removal of quasiperiodic noise using frequency domain statistics." *Journal of electronic imaging* 24, no. 1 (2015): 013003-013003. https://doi.org/10.1117/1.JEI.24.1.013003
[40] Sur, Frédéric. "An a-contrario approach to quasi-periodic noise removal." In *2015 IEEE International Conference on Image Processing (ICIP)*, pp. 3841-3845. IEEE, 2015. https://doi.org/10.1109/ICIP.2015.7351524
[41] Varghese, Justin, Saudia Subash, Nasser Tairan and Bijoy Babu. "Laplacian-based frequency domain filter for the restoration of digital images corrupted by periodic noise." *Canadian journal of electrical and computer engineering* 39, no. 2 (2016): 82-91. https://doi.org/10.1109/CJECE.2015.2490598
[42] Varghese, Justin, Saudia Subash and Nasser Tairan. "Fourier transform-based windowed adaptive switching minimum filter for reducing periodic noise from digital images." *IET image processing* 10, no. 9 (2016): 646-656. https://doi.org/10.1049/iet-ipr.2015.0750
[43] Grediac, Michel, Frédéric Sur and Benoît Blaysat. "Removing quasi-periodic noise in strain maps by filtering in the Fourier domain." *Experimental Techniques* 40 (2016): 959-971. https://doi.org/10.1007/s40799-016-0100-2
[44] Varghese, Justin. "Adaptive threshold based frequency domain filter for periodic noise reduction." *AEU-international journal of electronics and communications* 70, no. 12 (2016): 1692-1701. https://doi.org/10.1016/j.aeue.2016.10.008
[45] Varghese, J. "Frequency-domain-based switching median filter for the restoration of images corrupted with high-density periodic noise." *Scientia Iranica* 24, no. 3 (2017): 1312-1324. https://doi.org/10.24200/sci.2017.4114
[46] Zhou, Weirong, Yunjie Zhang and Yongchao Liu. "Bilateral linear operator for period noise image De-noising." In *Proceedings of the 2nd International Conference on Computer Science and Application Engineering*, pp. 1-5. 2018. https://doi.org/10.1145/3207677.3277978
[47] Chakraborty, Debolina, Anirban Chakraborty, Ayan Banerjee and Sekhar R. Bhadra Chaudhuri. "Automated spectral domain approach of quasi-periodic denoising in natural images using notch filtration with exact noise profile." *IET image processing* 12, no. 7 (2018): 1150-1163. https://doi.org/10.1049/iet-ipr.2017.0307
[48] Ketenci, Seniha and Ali Gangal. "Automatic reduction of periodic noise in images using adaptive Gaussian star filter." *Turkish Journal of Electrical Engineering and Computer Sciences* 25, no. 3 (2017): 2336-2348. https://doi.org/10.3906/elk-1506-78
[49] Ionita, M. and H. Coanda. "Wavelet and Fourier decomposition based periodic noise removal in microscopy images." *Sci. Bulletin Electr. Eng. Faculty* 38, no. 1 (2018): 68-71. https://doi.org/10.1515/sbeef-2017-0025
[50] Varghese, Justin, Saudia Subhash, Kamalraj Subramaniam and Kuttaiyur Palaniswamy Sridhar. "Adaptive Gaussian notch filter for removing periodic noise from digital images." *IET Image Processing* 14, no. 8 (2020): 1529-1538. https://doi.org/10.1049/iet-ipr.2018.5707
[51] Ali, Ahmad Ali Imran Mohd, Shahrizan Jamaludin, Md Mahadi Hasan Imran, Ahmad Faisal Mohamad Ayob, Sayyid Zainal Abidin Syed Ahmad, Mohd Faizal Ali Akhbar, Mohammed Ismail Russtam Suhrab and Mohamad Riduan Ramli. "Computer vision and image processing approaches for corrosion detection." *Journal of Marine Science and Engineering* 11, no. 10 (2023): 1954. https://doi.org/10.3390/jmse11101954
[52] Sakti, Arya Mahendra, Riandadari, Dyah, Ganda andita Nataria Fitri, Abdi, Ferly Isnomo, Utama, Firman Yasa, Wulandari, Diah, Sulaiman, Abdul Mudjib and Puspitasari, Dewi. "Corrosion morphological characteristics of the blackening process on plate and cylindrical workpieces." *Journal of Advanced Research in Applied Sciences and Engineering Technology 56*, no. 1 (2026): 100-108. https://doi.org/10.37934/araset.56.2.102110

[53] Subeki, Nur, Achmad Fauzan Hery Soegiharto andi Firkriyanto and Nadiaseptria Gidiazalia. "Crack Propagation Analysis of Fatigue Due to External Corrosion on the Construction of the Ferris Wheel in Alun-Alun Kota Batu." *Journal of Advanced Research in Applied Mechanics* 111, no. 1 (2023): 62-73. https://doi.org/10.37934/aram.111.1.6273